CHEMISTRY OF MATERIALS

ARTICLE

pubs.acs.org/cm

Nonlinear Optical Switching Behavior in the Solid State: A Theoretical Investigation on Anils

Audrey Ségerie,[†,‡] Frédéric Castet,[†] Mohamed Benali Kanoun,[‡,§] Aurélie Plaquet,[†,‡] Vincent Liégeois,[‡] and Benoît Champagne*[,‡]

[†]Université de Bordeaux, Institut des Sciences Moléculaires (UMR 5255 CNRS), cours de la Libération, 351, F-33405 Talence, France

[‡]Laboratoire de Chimie Théorique, Unité de Chimie Physique Théorique et Structurale, Facultés Universitaires Notre-Dame de la Paix (FUNDP), rue de Bruxelles 61, B-5000 Namur, Belgium

Supporting Information

ABSTRACT: The linear ($\chi^{(1)}$) and second-order nonlinear ($\chi^{(2)}$) optical properties of two anil crystals, [*N*-(4-hydroxy)-salicylidene-amino-4-(methylbenzoate) and *N*-(3,5-di-*tert*-butylsalicylidene)-4-aminopyridine, denoted **4A** and **4P**, respectively], as well as the optical contrasts upon switching between their enol (E) and keto (K) forms, have been investigated by combining the molecular responses calculated using quantum chemistry methods and an electrostatic interaction scheme to account for the local field effects. It is found that intermolecular interactions impact differently the K/E optical contrasts in the two systems, which illustrates the importance of the supramolecular organization on the macroscopic responses. In **4A**, the surrounding effects on the (hyper)polarizabilities are similar in the enol and keto forms, leading to optical contrasts very close to those of the isolated molecule. In contrast, an enhancement of the second-order susceptibility is observed in the keto form of **4P**, leading to a large $\chi^{(2)}(\mathbf{K})/\chi^{(2)}(\mathbf{E})$ contrast. Moreover, the $\chi^{(2)}(\mathbf{4A})/\chi^{(2)}(\mathbf{4P})$ ratio for the most stable enol forms is obtained to be in good agreement with previous experimental investigations, which supports the reliability of the computational procedure.

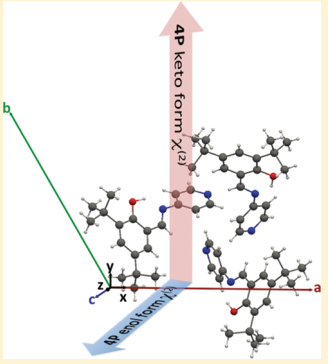

KEYWORDS: nonlinear optics, organic molecular crystals, keto−enol molecular switches, first hyperpolarizabilities, second-order nonlinear optical susceptibilities, quantum chemical calculations, electrostatic interaction schemes

I. INTRODUCTION

Designing materials with controlled switching abilities constitutes an important step toward new storing devices such as optical memories.[1] Among these, photochromic materials possessing commutable nonlinear optical (NLO) responses are particularly attractive, because the nonresonant character of NLO enables the reading of the stored information outside the absorption band, so that erasure during reading can be avoided. At the molecular level, a large variety of NLO switches exhibiting large changes in their NLO responses have been designed during the past 15 years.[2,3] Molecular crystals exhibiting such large contrasts of second-order NLO responses are the focus of the present investigation.

Efficient NLO switches have to achieve several conditions: (i) the molecules constituting the crystal must display large NLO responses, (ii) the change of NLO properties upon switching should be substantial, and (iii) inherently to the first hyperpolarizabilities (β) or the second-order NLO susceptibilities ($\chi^{(2)}$), the molecules and the crystal should be noncentrosymmetric. The conservation of the molecular properties at the macroscopic scale is already a challenge. Indeed, it is often difficult to obtain noncentrosymmetric crystals[4] from molecules having large first hyperpolarizability, because these molecules are in general donor−acceptor systems with large dipole moments that favor antiparallel stacking and centrosymmetric crystallization. This is why several strategies have been adopted to avoid the unfavorable arrangements: for example, chemical modifications of the molecules can be realized in order to force the alignment of the dipoles during crystallization,[5] or to reduce the dipoles in such a way that other intermolecular interactions govern the molecular packing. This molecule and crystal design is often a complex and long procedure that can be accelerated by theoretical modeling, because of its ability to predict the NLO properties and to interpret these in terms of the molecular structures,[6] even before experimental investigations.

Although several theoretical studies have been performed to rationalize the switching NLO properties of push−pull π-conjugated systems in solutions,[3d−f,i,j] their properties in the solid state, to our knowledge, have not yet been analyzed, which makes the design of efficient switching molecular crystals incomplete. Therefore, this paper intends to address this missing step by evaluating and analyzing the second-order NLO properties of molecular crystals, going from the molecular properties to those of the crystals via those of the unit cell. This is carried out by considering two anil derivatives: *N*-(4-hydroxy)-salicylidene-amino-4-(methylbenzoate) and *N*-(3,5-di-*tert*-butylsalicylidene)-4-aminopyridine, denoted

Received: June 1, 2011
Revised: July 4, 2011
Published: August 09, 2011

according to ref 7, **4A** and **4P**, respectively. These compounds have been shown to switch between an enol-imine form (E) and a keto-amine form (K) by an intramolecular proton transfer. Their noncentrosymmetric crystal packing ensures nonzero second-order NLO susceptibilities that have been investigated experimentally, including their switching,[8] in addition to complementary studies of their linear and nonlinear optical responses in solutions.[9] The high efficiency of this solid state switch is provided by the small geometric distortions associated with the photoinduced reactions, which ensure a good fatigue resistance to the material.

The major steps of the theoretical and computational approaches are summarized in section II, highlighting the aspects that are specific to the current systems. Then, in section III, the results of the linear and second-order NLO responses are successively analyzed for the crystals, molecules, and unit cells with an emphasis on the evolution of the responses along the tautomeric equilibrium. Further discussions including comparisons with experiments are then carried out.

II. THEORY, METHODS OF CALCULATION, AND CRYSTALS STRUCTURES

II.A. Definitions of the Linear and Nonlinear Responses. Here, linear and nonlinear optical phenomena correspond to those molecular properties related to the successive responses of the dipole moment to an external electric field $E(\omega)$:

$$\mu = \mu_0 + \alpha E(\omega) + \frac{1}{2}\beta E^2(\omega) + \frac{1}{6}\gamma E^3(\omega) + \ldots \quad (1)$$

where μ_0 is the permanent dipole moment, α the polarizability, β the first hyperpolarizability, and γ the second hyperpolarizability. At the crystal or macroscopic level, the analog quantity to μ is the electric polarization, which can also be expanded in a power series of the electric field:

$$P = P_0 + \varepsilon_0[\chi^{(1)}E(\omega) + \chi^{(2)}E^2(\omega) + \chi^{(3)}E^3(\omega) + \ldots] \quad (2)$$

Thus, P_0 is the permanent polarization—or the permanent electric dipole moment per unit volume—$\chi^{(1)}$ is the (linear) optical susceptibility while $\chi^{(2)}$ and $\chi^{(3)}$ are the second- and third-order NLO susceptibilities, respectively. It is common practice to use the molecular responses as a starting point to evaluate their macroscopic analogs, but many effects can lead to substantial variations.

II.B. From Molecular to Crystal Properties: Electrostatic Interaction Schemes. Several methods have been developed in order to determine the macroscopic optical properties,[10] of which the simplest is the oriented gas model, due to Chemla et al.[11] In that method, the $\chi^{(n)}$ quantities are calculated from simple tensor sums of the (hyper)-polarizabilities of the molecules constituting the elementary unit cell. Corrective factors can then be added in a second step to account for the effects of local electric fields. The relevance of this method is ensured provided the intermolecular interactions are weak, while the macroscopic responses are strongly dependent on the values of local field factors. More sophisticated schemes take into account the intermolecular interactions. They include the "supermolecule" model,[12] where an aggregate of molecules is considered as a giant molecule, but this approach is limited to small-size aggregates and the long-range interactions are truncated. On the other hand, the later are included when resorting to crystalline orbitals treatment, which assumes an infinite periodic system and accounts for all types of interactions.[13]

In our work, we employ the electrostatic interaction scheme proposed by Munn and Hurst,[14] which is based on the Rigorous Local Field Treatment (RLFT)[15] to evaluate the macroscopic linear and nonlinear optical susceptibilities from molecular responses calculated using quantum chemistry methods. The linear optical susceptibility tensor for a crystal with Z molecules labeled k (or Z submolecules labeled kj) per unit cell with a volume V reads

$$\vec{\vec{\chi}}^{(1)} = \frac{1}{\varepsilon_0 V}\sum_{kj}^{Z}\vec{\vec{\alpha}}_{kj}\vec{\vec{d}}_{kj} = \sum_{kj,k'j'}\left[\left(\frac{\vec{\vec{\alpha}}}{\varepsilon_0 V}\right)^{-1} - \vec{\vec{L}}\right]^{-1}_{kj,k'j'} \quad (3)$$

where $\vec{\vec{d}}_{kj}$ is the 3×3 local field tensor, given by

$$\vec{\vec{d}}_{kj} = \sum_{k'j'}\left[\vec{\vec{I}} - \frac{\vec{\vec{L}}\,\vec{\vec{\alpha}}}{\varepsilon_0 V}\right]^{-1}_{kj,k'j'} \qquad with\ \vec{\vec{\alpha}}_{kj,k'j'} = \vec{\vec{\alpha}}_{kj}\delta_{kk'}\delta_{jj'} \quad (4)$$

$\vec{\vec{\alpha}}_{kj}$ is the polarizability tensor for submolecule kj and $\vec{\vec{I}}$ is a unit tensor of order $3Z \times 3Z$ with 3×3 subtensors $\vec{\vec{I}}\delta_{kj,k'j'}$. The interactions between one molecule (or submolecule) of the reference unit cell and the infinite number of equivalent molecules (or submolecules) of the crystals are described with the Lorentz-factor tensor $\vec{\vec{L}}$. The summation of the dipole lattice is realized with the Ewald method,[15] which presents the advantage of ensuring a rapid convergence of the sums in the reciprocal space. For example, $\vec{\vec{L}}_{kj,k'j'}$ expresses the induced field at molecule k (or submolecule kj) of the reference unit cell caused by the induced dipole moments on all k' molecules (or $k'j'$ submolecules). Via a matrix inversion, this approach enables the self-consistency of the interactions between the field-induced dipole moments. The second-order NLO susceptibility tensor then reads:

$$\vec{\vec{\chi}}^{(2)}(-\omega;\omega_1,\omega_2) = \frac{1}{2\varepsilon_0 V}\sum_{kj}^{Z}\vec{\vec{\beta}}_{kj}(-\omega;\omega_1,\omega_2)[\vec{\vec{d}}_{kj}(\omega_2)\vec{\vec{d}}_{kj}(\omega_1)\vec{\vec{d}}_{kj}(\omega)] \quad (5)$$

where $\vec{\vec{\beta}}_{kj}$ is the first hyperpolarizability tensor of submolecule kj and $\omega = \omega_1 + \omega_2$. This approach has been employed broadly for obtaining the linear and nonlinear susceptibilities of molecular crystals.[16] In this study, our interest is focused on the second harmonic generation (SHG) phenomenon characterized by $\omega_1 = \omega_2$ and, in particular, for $\lambda = 1907$ nm, because the experiments on **4A** and **4P** have been performed at this wavelength.[7] The molecular responses employed in eqs 3−5 were evaluated quantum mechanically.

II.C. Quantum Chemical Evaluation of the Molecular Properties. The geometry optimizations of the molecular structures were carried out at the density functional theory (DFT) level of approximation, using the B3LYP exchange-correlation functional and the 6-311G(d) basis set. The components of the static molecular responses, the α and β tensors, were determined with the coupled-perturbed Hartree−Fock approach (CPHF), the static equivalent to the time-dependent Hartree−Fock (TDHF) method,[17] and with the density functional theory (DFT). In the latter case, we used the B3LYP exchange-correlation (XC) and the long-range corrected LC-BLYP[18,19] functionals. The dynamic α and β tensors of the **4A** and **4P** molecules were calculated using TDHF or within the time-dependent density functional theory (TDDFT)[20] by employing the same XC functionals. At both levels of approximation, these calculations were performed employing the 6-311+G(d) basis set including diffuse and polarization basis functions, to properly describe the electronic (hyper)polarizations with a good compromise between accuracy and computational costs. To account more precisely for electron correlation effects, we also carried out calculations using the Møller−Plesset second-order (MP2) theory, as well as the 6-31G(d) and 6-31+G(d) basis sets, in combination with the finite field approach.[21] The accuracy of the numerical derivatives was improved by adopting the Romberg procedure. To include both electron correlation and dispersion effects, the dynamic α and β tensors were calculated by employing the multiplicative scheme, which consists in correcting the static MP2 values by the TDHF/CPHF ratio. The same approaches were adopted to evaluate the α and β tensors of the unit cell,

dx.doi.org/10.1021/cm2015516 |Chem. Mater. 2011, 23, 3993–4001

Scheme 1. (Left) Molecular Structure of 4A and 4P in Their Enol Form; (Right) Representation of the Unit Cells of 4A−E (Top) and 4P−E (Bottom) in Their Molecular (*x*-, *y*-, *z*-Axes) and Crystalline Frame (*a*-, *b*-, *c*-Axes)[a]

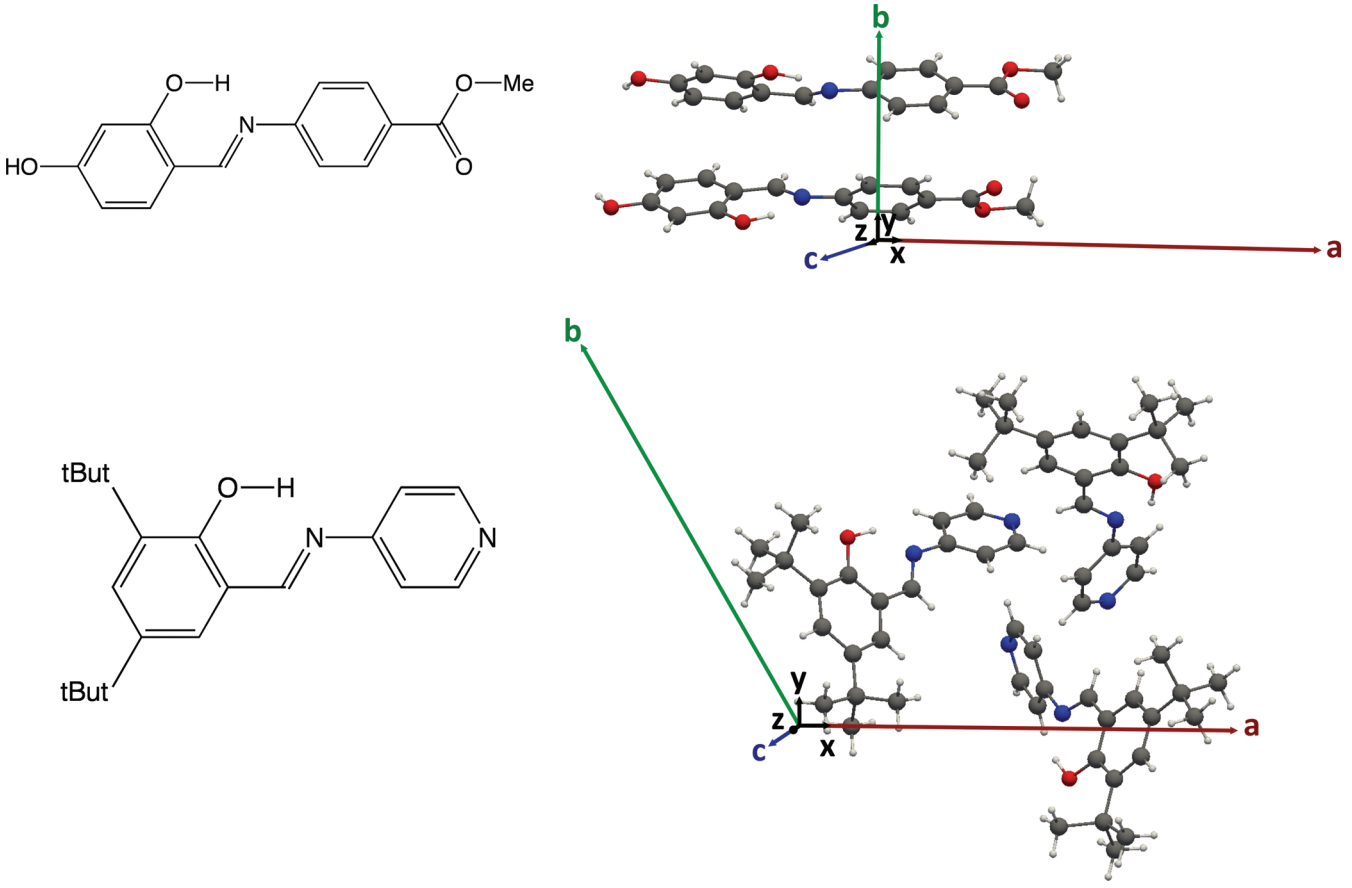

[a] As obtained from X-ray data.[24]

except MP2, for obvious computational reasons. All calculations were performed using the Gaussian 03 and 09 quantum chemistry packages.[22,23]

II.D. Crystal Structures. The crystal structures of **4A** and **4P**[7] are a prerequisite to determine the linear and nonlinear macroscopic properties of the crystals and of the unit cells. The **4A**−**E** crystal is monoclinic with space group *Pc*, there are two molecules per unit volume ($Z = 2$), and the unit-cell parameters are $a = 14.739$ Å, $b = 7.027$ Å, $c = 6.096$ Å, $\alpha = 90°$, $\beta = 99.21°$, and $\gamma = 90°$. **4P**−**E** belongs to the trigonal space group $P3_2$ with $Z = 3$ and the unit-cell parameters $a = b = 16.002$ Å, $c = 6.040$ Å, $\alpha = \beta = 90°$, and $\gamma = 120°$. The following expressions provide the relation between the molecular and crystalline axes of **4A** and **4P**, respectively: $\vec{a} = 14.74\vec{x}$, $\vec{b} = 7.03\vec{y}$, $\vec{c} = -0.98\vec{x} + 6.02\vec{z}$, and $\vec{a} = 16.00\vec{x}$, $\vec{b} = -8.00\vec{x} + 13.86\vec{y}$, $\vec{c} = 6.04\vec{z}$. The molecular structures, the unit cells, and the two axes systems are sketched in Scheme 1, showing that the crystal packing is much different in **4A** and **4P**. Indeed, in **4A**, the two molecules of the unit cell are roughly parallel whereas the three molecules of **4P** are positioned around a 3-fold axis and, thus, are differently oriented.

For the enol-imine forms (crystals as well as unit cells), we used the crystallographic data determined by X-ray diffraction (XRD) experiments. On the other hand, the crystallographic structure of the keto-amine forms could not be probed by XRD, because of their instability, so that, to build the corresponding crystal structures, we assumed that the intramolecular proton transfer leads to a negligible change of the unit-cell parameters. This is justified by the fact that the switching in the crystalline state is possible, because of the weak geometrical distortions associated with the photoinduced reaction.[25] Therefore, in this work, the unit cell of both the enol-imine and keto-amine forms of **4A** and **4P** were built from the enol-amine XRD data. First, the molecular geometry of both the K and E forms was optimized using density functional theory (DFT) at the B3LYP/6-311G(d) level. In this step, we kept the average orientation of the molecule in the crystal, preventing a reorientation along the main inertial axes. Once the geometry was optimized, we applied the set of symmetry operations characteristic to the space group to rebuild the entire unit cell. These operations were performed in the crystal axes system.

II.E. Implementation of the Classical Approach to Evaluate the Local Field Tensors. Following the calculation of the molecular properties, the local field tensors (eq 4) were determined after distributing the polarizabilities over molecular sites. Similar distributions of the polarizabilities and first hyperpolarizabilities were also applied to get $\chi^{(1)}$ and $\chi^{(2)}$ from eqs 3 and 5. Different partitioning schemes of the molecular properties were adopted and are illustrated in Figures S1 and S2 in the Supporting Information. These take into account the chemical composition—and the presence of functional groups—of the molecules and are based on the RLFT$_n$ model, where n is the number of submolecules per molecule. Therefore, on the one hand, the RLFT$_1$ scheme considers the molecule as a single dipole situated at the center of mass while, on the other hand, in the RLFT$_{20}$ and RLFT$_{23}$ schemes, the molecules **4A** and **4P** are divided into 20 and 23 polarizable sites placed on each heavy atoms, respectively.

III. RESULTS AND DISCUSSIONS

III.A. Linear and Nonlinear Macroscopic Responses of the 4A and 4P Crystals. The linear and second-order nonlinear

Table 1. Diagonal $\chi^{(1)}$ Tensor Components (Pure Numbers, λ = 1907 nm) and Keto/Enol $\chi^{(1)}$ Contrasts for 4A and 4P, as Determined at Different Levels of Approximation, Using the Polarizability Distribution over All the Non-Hydrogen Atoms

		HF/ 6-311+G(d)	LC-BLYP/ 6-311+G(d)	MP2/ 6-31+G(d)
4A−E	$\chi^{(1)}_{xx}$	2.681	2.873	3.049
	$\chi^{(1)}_{yy}$	1.035	1.038	1.088
	$\chi^{(1)}_{zz}$	1.679	1.773	1.865
4A−K	$\chi^{(1)}_{xx}$	3.006	3.371	3.798
	$\chi^{(1)}_{yy}$	0.904	0.892	0.940
	$\chi^{(1)}_{zz}$	1.796	1.896	2.015
Contrasts	$\chi^{(1)}_{xx}(\mathbf{K})/\chi^{(1)}_{xx}(\mathbf{E})$	1.12	1.17	1.25
	$\chi^{(1)}_{yy}(\mathbf{K})/\chi^{(1)}_{yy}(\mathbf{E})$	0.87	0.86	0.86
	$\chi^{(1)}_{zz}(\mathbf{K})/\chi^{(1)}_{zz}(\mathbf{E})$	1.07	1.07	1.08
4P−E	$\chi^{(1)}_{xx} = \chi^{(1)}_{yy}$	1.516	1.574	1.632
	$\chi^{(1)}_{zz}$	1.631	1.694	1.767
4P−K	$\chi^{(1)}_{xx} = \chi^{(1)}_{yy}$	1.814	1.972	2.209
	$\chi^{(1)}_{zz}$	2.359	2.662	3.123
Contrasts	$\chi^{(1)}_{xx}(\mathbf{K})/\chi^{(1)}_{xx}(\mathbf{E})$	1.20	1.25	1.35
	$\chi^{(1)}_{zz}(\mathbf{K})/\chi^{(1)}_{zz}(\mathbf{E})$	1.45	1.57	1.77

Table 2. Refractive Indices (Pure Numbers, λ = 1907 nm) of 4A and 4P Crystals along the *x*-, *y*-, and *z*-Axes, as Determined at Different Levels of Approximation Using the Polarizability Distribution over All the Non-Hydrogen Atoms

		HF/ 6-311+G(d)	LC-BLYP/ 6-311+G(d)	MP2/ 6-31+G(d)
4A−E	n_x	1.919	1.968	2.012
	n_y	1.427	1.428	1.445
	n_z	1.637	1.665	1.693
4A−K	n_x	2.001	2.091	2.190
	n_y	1.380	1.375	1.393
	n_z	1.672	1.702	1.736
4P−E	$n_x = n_y$	1.586	1.604	1.622
	n_z	1.622	1.641	1.663
4P−K	$n_x = n_y$	1.677	1.724	1.791
	n_z	1.833	1.914	2.031

susceptibilities of **4A** and **4P** were calculated within the RLFT scheme. The data for different combinations of (hyper)polarizability partitionings and levels of approximation are presented and discussed in detail in the Supporting Information. The main conclusions are (i) the dipolar or $RLFT_1$ approximation is not sufficient to describe the linear and nonlinear effects; (ii) partitioning the molecular properties on five (**4A**) or six (**4P**) molecular chemical groups already leads to $\chi^{(1)}$ and $\chi^{(2)}$ values, in good agreement with the more-evolved scheme where the (hyper)-polarizabilities are distributed on all non-hydrogen atoms; (iii) corresponding $\chi^{(1)}$ and $\chi^{(2)}$ tensor components present similar variations with the method of calculations; (iv) diffuse functions are important in several cases, especially for the $\chi^{(2)}$ responses; and (v) there is a good agreement between the $\chi^{(1)}$ and $\chi^{(2)}$ tensor components evaluated from LC-BLYP and MP2 (hyper)-polarizabilities, whereas the HF and B3LYP methods usually lead to smaller and larger linear and nonlinear susceptibilities, respectively. These relative values of the $\chi^{(1)}$ and $\chi^{(2)}$ tensor components are corroborated by several investigations on the effects of electron correlation on the (hyper)polarizabilities as well as on the performance of the DFT schemes with more or less conventional exchange-correlation functionals.[19,26] Following these studies, for most cases, both the MP2 and LC-BLYP data are selected to assess the chemical and surrounding effects on $\chi^{(1)}$ and $\chi^{(2)}$. Although to a lower extent, the HF data are also primarily considered, since they are used to account for the frequency dispersion effects on the MP2 results. All linear and nonlinear macroscopic tensor components discussed in the paper have been obtained for λ = 1907 nm using the finest $RLFT_{20}$ (**4A**) and $RLFT_{23}$ (**4P**) distribution schemes. To facilitate comparisons between the $\chi^{(1)}$ and $\chi^{(2)}$ tensor components and their microscopic α and β analogs, all components are given in the molecular frames (*x*-, *y*-, *z*- axes; see Scheme 1).

The $\chi^{(1)}$ diagonal tensor components of both tautomeric forms of **4A** and **4P** are listed in Table 1, together with the $\chi^{(1)}(\mathbf{K})/\chi^{(1)}(\mathbf{E})$ ratios. For the enol and keto forms of **4A**, $\chi^{(1)}_{xx} > \chi^{(1)}_{zz} > \chi^{(1)}_{yy}$ while for **4P**, $\chi^{(1)}_{zz} > \chi^{(1)}_{xx}$ and $\chi^{(1)}_{xx} = \chi^{(1)}_{yy}$ by symmetry. This is obtained at all levels of approximation and for both the static and dynamic responses (see Tables S1 and S2 in the Supporting Information). Moreover, the keto form presents a larger linear susceptibility than the enol form, especially for **4P**, where the $\chi^{(1)}(\mathbf{K})/\chi^{(1)}(\mathbf{E})$ ratio reaches 1.77 at the MP2/6-31+G(d) level. In addition, **4A** presents larger $\chi^{(1)}$ values than **4P**, for both tautomeric forms. Subsequently, the refractive indices have been determined from $n = [\chi^{(1)} + 1]^{1/2}$ (see Table 2). Considering the MP2/6-31+G(d) values, the refractive indices n_x, n_y, and n_z vary by +9%, −4%, and +3%, respectively, upon switching **4A** from the enol to the keto form. In the case of **4P**, the variations amount, in the same order, to +10% for n_x and n_y and +22% for n_z.

Table 3 lists the dominant $\chi^{(2)}$ tensor components, as well as the associated $\chi^{(2)}(\mathbf{K})/\chi^{(2)}(\mathbf{E})$ ratios. In the **4A** crystal, $\chi^{(2)}_{xxx}$ is the dominant tensor component, as could be understood from the orientation of the molecules in the unit cells. All $\chi^{(2)}_{xxx}(\mathbf{K})/\chi^{(2)}_{xxx}(\mathbf{E})$ contrasts are smaller than unity and range between 0.46 when using MP2 data to 0.77 at the HF and LC-BLYP levels. As shown in Table S3 in the Supporting Information, these contrasts are almost constant in the $h\upsilon$ = 0−0.60 eV (∞−1907 nm) range, whereas the use of a simplified distribution scheme leads to typical increases of the contrasts by 10% ($RLFT_{10}$) or decreases by 12%−17% ($RLFT_5$). For the **4A** crystal, the $\chi^{(2)}_{zxx}(\mathbf{K})/\chi^{(2)}_{zxx}(\mathbf{E})$ contrasts were also evaluated, since the $\chi^{(2)}_{zxx}$ tensor components are only 2−3 times smaller than the dominant component. In this case, the contrasts amount to 1.17 to 1.42, varying little from one method to another.

The situation is more complex in the **4P** crystal, since the relative amplitudes of the $\chi^{(2)}$ components change greatly when going from the enol to the keto forms. Indeed, in the enol form, $\chi^{(2)}_{zzz}$ is the largest component while the $\chi^{(2)}_{yyy}$ and $\chi^{(2)}_{zyy}$ components are 2−3 times smaller (also see Table S4 in the Supporting

dx.doi.org/10.1021/cm2015516 |*Chem. Mater.* 2011, 23, 3993–4001

Table 3. Dominant $\chi^{(2)}$ Tensor Components (pm/V, λ = 1907 nm) and Keto/Enol $\chi^{(2)}$ Contrasts, as Determined at Different Levels of Approximation, Using the (Hyper)polarizability Distribution over All the Non-Hydrogen Atoms

		HF/ 6-311+G(d)	LC-BLYP/ 6-311+G(d)	MP2/ 6-31+G(d)
4A−E	$\chi^{(2)}_{xxx}$	−26.882	−45.818	−66.475
	$\chi^{(2)}_{zxx}$	11.310	12.946	13.625
4A−K	$\chi^{(2)}_{xxx}$	−20.165	−35.340	−30.499
	$\chi^{(2)}_{zxx}$	16.005	16.131	15.912
Contrasts	$\chi^{(2)}_{xxx}$(K)/$\chi^{(2)}_{xxx}$(E)	0.75	0.77	0.46
	$\chi^{(2)}_{zxx}$(K)/$\chi^{(2)}_{zxx}$(E)	1.42	1.25	1.17
4P−E	$\chi^{(2)}_{yyy}$	1.948	2.260	3.001
	$\chi^{(2)}_{zyy}$	1.524	2.932	4.832
	$\chi^{(2)}_{zzz}$	3.332	5.860	8.656
4P−K	$\chi^{(2)}_{yyy}$	36.596	48.192	71.305
	$\chi^{(2)}_{zyy}$	15.496	26.246	−19.947
	$\chi^{(2)}_{zzz}$	20.583	26.647	−6.202
Contrasts	$\chi^{(2)}_{zzz}$(K)/$\chi^{(2)}_{zzz}$(E)	6.18	4.55	−0.72
	$\chi^{(2)}_{yyy}$(K)/$\chi^{(2)}_{zzz}$(E)	10.98	8.22	8.24

Information). On the other hand, for the keto form, the largest component is $\chi^{(2)}_{yyy}$ while the $\chi^{(2)}_{zyy}$ and $\chi^{(2)}_{zzz}$ components are smaller and their amplitude, with respect to $\chi^{(2)}_{yyy}$ is method dependent (see discussion in section III.B). Therefore, Table 3 lists the $\chi^{(2)}_{zzz}$(K)/$\chi^{(2)}_{zzz}$(E) and $\chi^{(2)}_{yyy}$(K)/$\chi^{(2)}_{zzz}$(E) contrasts, showing that the second-order NLO responses are, globally, much larger for the keto form than for the enol form. Besides, one notes that the $\chi^{(2)}_{zyy}$ and $\chi^{(2)}_{zzz}$ components calculated at the MP2 level are negative, in contrast to those obtained at the HF and DFT levels, showing a significant impact of the method of calculation on the NLO responses. As discussed in the next sections, subtle electron correlation effects are related to the lack of strong donor/acceptor groups on the aromatic rings (and, thus, to the absence of a dominant charge-transfer direction) in the **4P** molecules, as well as to the nonparallel crystal packing.

Finally, the comparison between the macroscopic nonlinear responses of the two derivatives exhibits higher values for the **4A**−**E** than for the **4P**−**E** crystal. This theoretical result—which, contrary to experiment, also presents the advantage of predicting the sign of the nonlinear susceptibility tensor components—can be correlated with powder second harmonic generation (SHG) measurements realized by Sliwa et al.,[7] where the SHG intensities of **4A**−**E** and **4P**−**E** are, respectively, 10 and 3 times larger than that of urea. To gain further insight on all these results, calculations were performed on the **4A** and **4P** isolated molecules, as well as on their crystal unit cells.

III.B. Molecular Polarizabilities and First Hyperpolarizabilities. The main tensor components of the dynamic molecular properties in the molecular frames are listed in Tables 4 and 5. The β_{vec} values, corresponding to the norm of the (β_x, β_y, β_z) vector, where $\beta_i = {}^1/_3\Sigma_j(\beta_{ijj} + \beta_{jij} + \beta_{jji})$, are also given, since they provide information on the magnitude of β, in opposition to its orientation. In the case of **4A**, α_{xx} and β_{xxx} are the dominant

Table 4. Main Tensor Components of the Dynamic Polarizability (a.u., λ = 1907 nm) of 4A and 4P Molecules Calculated at Different Levels of Approximation

		HF/ 6-311+G(d)	LC-BLYP/ 6-311+G(d)	MP2/ 6-31+G(d)
4A-E	α_{xx}	340.30	358.81	375.10
	α_{yy}	110.98	111.09	114.70
	α_{zz}	175.27	181.69	187.62
4A-K	α_{xx}	368.29	399.99	434.15
	α_{yy}	101.53	100.63	104.20
	α_{zz}	185.78	192.59	200.04
Contrasts	α_{xx}(K)/α_{xx}(E)	1.08	1.11	1.16
	α_{yy}(K)/α_{yy}(E)	0.91	0.91	0.91
	α_{zz}(K)/α_{zz}(E)	1.06	1.06	1.07
4P-E	α_{xx}	242.28	247.77	253.82
	α_{yy}	253.56	261.05	267.03
	α_{zz}	267.61	275.41	283.64
4P−K	α_{xx}	257.58	267.28	279.28
	α_{yy}	262.24	270.04	278.20
	α_{zz}	278.66	291.84	308.15
Contrasts	α_{xx}(K)/α_{xx}(E)	1.06	1.08	1.10
	α_{yy}(K)/α_{yy}(E)	1.03	1.03	1.04
	α_{zz}(K)/α_{zz}(E)	1.04	1.06	1.09

components, which is a natural consequence of the alignment of the charge transfer (CT) direction of the chromophore with the *x*-axis. For the polarizability, the next component, in decreasing order of magnitude, is α_{zz} (the molecular plane is almost parallel to the *xz*-plane), whereas, for the first hyperpolarizability, the next component is the off-diagonal β_{zxx} component. For α, the inclusion of electron correlation effects leads to a small increase (5%−20%) of most components, whereas for β, the effect is stronger with an enhancement of β_{xxx} of the enol form by a factor of 2 when going from HF to MP2. This enhancement of 100% of the β values due to electron correlation effects is typical and is in good agreement with other investigations.[26c] The modifications of β_{xxx} of the keto form are smaller. Comparisons between the different levels of approximation are further provided in Figure S3 in the Supporting Information, demonstrating a consistent view on the orientation of the β vector, with respect to the molecular frame. As a matter of fact, the β_{xxx}(K)/β_{xxx}(E) ratio ranging from 0.40 using MP2 to 0.71 ± 0.02 at the HF and LC-BLYP levels can already account for the amplitude of the $\chi^{(2)}_{xxx}$(K)/$\chi^{(2)}_{xxx}$(E) ratio (equal to 0.46, 0.75, and 0.77 at the MP2, HF, and LC-BLYP levels of approximation, respectively) in **4A**. A similar conclusion can be drawn on the α_{ii}(K)/α_{ii}(E) ratios (where i = *x*, *y*, or *z*), as indicative of the $\chi^{(1)}_{xx}$(K)/$\chi^{(1)}_{xx}$(E) ratios.

The diagonal components of the polarizability tensor of the **4P** molecule are very similar but follow the same $\alpha_{zz} > \alpha_{yy} > \alpha_{xx}$ trend as in the crystal. Its β-tensor is not dominated by a single charge-transfer component, because of the lack of strong donor and/or acceptor groups on the aromatic rings. For the enol form, the β_{zzz} and β_{yzz} components are the largest, as determined at all

dx.doi.org/10.1021/cm2015516 |*Chem. Mater.* 2011, 23, 3993–4001

Table 5. Main Tensor Components of the Dynamic First Hyperpolarizability (a.u., λ = 1907 nm) of 4A and 4P Molecules Calculated at Different Levels of Approximation

		HF/ 6-311+G(d)	LC-BLYP/ 6-311+G(d)	MP2/ 6-31+G(d)
4A−E	β_{xxx}	−2152.4	−3328.0	−4469.0
	β_{zxx}	791.4	937.7	1010.0
	β_{vec}	2194.7	3421.3	4620.6
4A−K	β_{xxx}	−1579.0	−2286.0	−1789.9
	β_{zxx}	948.7	922.4	798.1
	β_{vec}	1791.5	2347.1	1782.6
Contrasts	β_{xxx}(K)/β_{xxx}(E)	0.73	0.69	0.40
	β_{zxx}(K)/β_{zxx}(E)	1.20	0.98	0.79
4P−E	β_{zzz}	395.4	646.3	900.0
	β_{yyy}	1.68	−80.3	−27.5
	β_{yzz}	−371.2	−461.4	−525.8
	β_{vec}	930.0	1535.6	2063.0
4P−K	β_{zzz}	504.3	486.0	66.8
	β_{yyy}	74.5	149.2	244.4
	β_{yzz}	−495.0	−450.1	−253.1
	β_{vec}	1105.0	1005.3	344.5
Contrasts	β_{zzz}(K)/β_{zzz}(E)	1.28	0.75	0.07
	β_{yyy}(K)/β_{zzz}(E)	0.19	0.23	0.27

levels of approximation (also see Table S5 in the Supporting Information), while for the keto tautomer, the MP2/6-31+G(d) results are different and predict a strong reduction of the β_{zzz} component while β_{vec} is reduced by a factor of ∼3. This dependence of the orientation of the β-vector, as a function of the method of calculation (Figure S3 in the Supporting Information), was already noted in a previous investigation.[9a] Therefore, for our purposes, we concentrate on using the MP2 results, together with frequency dispersions estimated within the TDHF method. Considering the individual molecules, the β_{yyy}(K)/β_{zzz}(E) ratios are much different from the $\chi^{(2)}_{yyy}$(K)/$\chi^{(2)}_{zzz}$(E) ratios, and are more than 1 order of magnitude smaller. The presence of three **4P** molecules per unit cell and their relative position (Scheme 1) is postulated as an explanation for the difference between the β(K)/β(E) and $\chi^{(2)}$(K)/$\chi^{(2)}$(E) ratios, whereas in the **4A** unit cell, the CT axes of the two molecules are almost parallel.

Moreover, consistently with the linear susceptibility differences, the keto forms present larger polarizability than the corresponding enol forms, which can be related to the smaller excitation energy value of the dipole-allowed low-energy optical transition.[9b]

III.C. Linear and Nonlinear Optical Responses of the Unit Cells. As a next step, the (hyper)polarizabilities of the unit cells were determined. Tables 6 and 7 report their TDHF/6-311+G(d) and LC-BLYP/6-311+G(d) dynamic polarizabilities and first hyperpolarizabilities, as well as the $\alpha/\varepsilon_0 V$ and $\beta/2\varepsilon_0 V$ quantities, which are the unit-cell analogs of the crystal linear and nonlinear susceptibilities, respectively.

Table 6. Tensor Components of the Dynamic Polarizability Calculated at the TDHF/6-311+G(d) and LC-BLYP/6-311+G(d) Levels (λ = 1907 nm) for the Unit Cells of 4A and 4P[a]

		HF/6-311+G(d)		LC-BLYP/6-311+G(d)	
		α	$\alpha/\varepsilon_0 V$	α	$\alpha/\varepsilon_0 V$
4A−E	α_{xx}	600.87	1.795	631.74	1.888
	α_{yy}	227.85	0.681	229.88	0.687
	α_{zz}	312.15	0.933	324.27	0.969
4A−K	α_{xx}	677.23	2.023	731.26	2.185
	α_{yy}	216.04	0.646	216.21	0.646
	α_{zz}	363.17	1.085	376.29	1.124
Contrasts	α_{xx}(K)/α_{xx}(E)	1.13	1.13	1.16	1.16
	α_{yy}(K)/α_{yy}(E)	0.95	0.95	0.94	0.94
	α_{zz}(K)/α_{zz}(E)	1.16	1.16	1.16	1.16
4P−E	α_{xx}	674.13	0.937	694.07	0.965
	α_{yy}	690.60	0.960	711.78	0.990
	α_{zz}	687.85	0.956	707.43	0.984
4P−K	α_{xx}	787.21	1.094	815.22	1.133
	α_{yy}	814.50	1.132	845.16	1.175
	α_{zz}	782.62	1.088	817.46	1.136
Contrasts	α_{xx}(K)/α_{xx}(E)	1.17	1.17	1.17	1.17
	α_{yy}(K)/α_{yy}(E)	1.18	1.18	1.19	1.19
	α_{zz}(K)/α_{zz}(E)	1.14	1.14	1.16	1.16

[a] α is given in a.u., and $\alpha/\varepsilon_0 V$ is a pure number.

Not surprisingly, the polarizability of the **4A** unit cell are consistent with those of the isolated molecules and of the crystals with $\alpha_{xx} > \alpha_{zz} > \alpha_{yy}$. Moreover, the α_{ii}(K)/α_{ii}(E) (i = x, y, or z) contrasts determined for the unit cell at the HF/6-311+G(d) and LC-BLYP/6-311+Gd) levels are in close agreement with, on the one hand, the molecular α_{ii}(K)/α_{ii}(E) ratios and, on the other hand, the crystal $\chi^{(1)}_{ii}$(K)/$\chi^{(1)}_{ii}$(E) ratios. In addition, from comparing data in Tables 1, 4, and 6, the parallel packing of a pair of **4A** molecules in the unit cell reduces the α_{xx} value per molecule consistently with simple electrostatics that predict a reduction of the electric field, because of the counteracting polarization effects. Indeed, going from one to two molecules, α_{xx} only increases by 76% (enol form) and by 84% (keto form).

Similar but amplified effects are observed in **4A** for β_{xxx} and β_{zxx}. So, β_{xxx} of the enol and keto tautomers increases by 39% and 59% upon forming the unit cell dimer, respectively. Moreover, the unit cell β_{xxx}(K)/β_{xxx}(E) contrast reaches 0.84 and 0.79 at the HF/6-311+G(d) and LC-BLYP/6-311+Gd) levels, in comparison with the values of 0.73 and 0.69 obtained for the isolated molecule (Table 5) and with the $\chi^{(2)}_{xxx}$(K)/$\chi^{(2)}_{xxx}$(E) ratio of 0.75 and 0.77 for the crystal (Table 3).

In the case of the **4P** derivative, as foreseen from the unit-cell spatial organization, the packing of the three **4P** molecules per unit cell is responsible for a change of the relative amplitudes in the diagonal polarizability tensor components. Contrary to the cases of the crystal and of the isolated molecule, where $\chi^{(1)}_{zz}$ and α_{zz} are, respectively, the major components, the α_{zz} component

dx.doi.org/10.1021/cm2015516 |Chem. Mater. 2011, 23, 3993–4001

Table 7. Tensor Components of the Dynamic First Hyperpolarizability Calculated at the TDHF/6-311+G(d) and LC-BLYP/6-311+G(d) Levels (λ = 1907 nm) for the Unit Cells of 4A and 4P[a]

		HF/6-311+G(d)		LC-BLYP/6-311+G(d)	
		β	$\beta/2\varepsilon_0 V$	β	$\beta/2\varepsilon_0 V$
4A−E	β_{xxx}	−3005.3	−8.731	−4624.7	−13.436
	β_{zxx}	1213.2	3.525	1427.5	4.147
4A−K	β_{xxx}	−2524.9	−7.336	−3634.9	−10.560
	β_{zxx}	1526.3	4.434	1469.4	4.269
Contrasts	β_{xxx}(K)/β_{xxx}(E)	0.84	0.84	0.79	0.79
	β_{zxx}(K)/β_{zxx}(E)	1.26	1.26	1.03	1.03
4P−E	β_{zzz}	871.8	1.179	1401.78	1.895
	β_{yyy}	564.2	0.763	689.51	0.932
	β_{zyy}	520.5	0.704	849.11	1.148
	β_{xyy}	137.0	0.185	177.80	0.240
4P−K	β_{zzz}	1231.2	1.664	1210.80	1.637
	β_{yyy}	1225.0	1.656	1312.67	1.774
	β_{zyy}	624.9	0.845	630.24	0.852
	β_{xyy}	513.7	0.694	483.92	0.654
Contrasts	β_{zzz}(K)/β_{zzz}(E)	1.41	1.41	0.86	0.86
	β_{yyy}(K)/β_{zzz}(E)	1.41	1.41	0.94	0.94

[a] β is given in a.u., and $\beta/2\varepsilon_0 V$ is given in units of pm/V.

Table 8. Keto/Enol Ratios of 4A and 4P for Systems Ranging from the Isolated Molecule and the Unit Cell to the Crystal, as Calculated at the LC-BLYP Level

	Molecule	Unit Cell	Crystal
	α_{uu}(K)/α_{uu}(E)	α_{uu}(K)/α_{uu}(E)	$\chi^{(1)}_{uu}$(K)/$\chi^{(1)}_{uu}$(E)
4A ($u = x$)	1.11	1.16	1.17
4P ($u = z$)	1.06	1.16	1.57
	β_{uuu}(K)/β_{uuu}(E)	β_{uuu}(K)/β_{uuu}(E)	$\chi^{(2)}_{uuu}$(K)/$\chi^{(2)}_{uuu}$(E)
4A ($u = x$)	0.69	0.79	0.77
4P ($u = z$)	0.75	0.86	4.55

is no longer the largest in the unit cell. For the first hyperpolarizability, the results show that $\beta_{zzz} > \beta_{yyy} \approx \beta_{zyy}$ when employing the HF method and with the LC-BLYP functional it becomes $\beta_{zzz} > \beta_{zyy} > \beta_{yyy}$ for the enol form and $\beta_{zzz} \approx \beta_{yyy} > \beta_{zyy}$ for the keto form. This leads to a β_{yyy}(K)/β_{zzz}(E) contrast of 1.41 (HF) and of 0.94 (LC-BLYP) for the unit cell that can be compared to the corresponding molecular contrast of 0.19 (HF) and 0.23 (LC-BLYP) (Table 5). In the crystal, the corresponding $\chi^{(2)}_{yyy}$(K)/$\chi^{(2)}_{zzz}$(E) contrast amounts to 10.98 (HF) and 8.22 (LC-BLYP) (see Table 3). This clearly demonstrates that, in **4P**, the surrounding effects—beyond the unit cell—have a large impact. The first hyperpolarizability vector calculated for the unit cells of **4A** and **4P** is sketched in Figure S4 in the Supporting Information.

IV. CONCLUSIONS

A systematic analysis of the keto/enol contrasts has been carried out for the dominant tensor components of the linear and nonlinear optical responses of two anil derivatives, *N*-(4-hydroxy)-salicylidene-amino-4-(methylbenzoate) and *N*-(3,5-di-*tert*-butylsalicylidene)-4-aminopyridine, denoted **4A** and **4P**, respectively. It is summarized in Table 8 for the isolated molecule, the unit cell, and the crystal. In **4A**, the small variations in the keto/enol ratios when moving from the molecule to the crystal demonstrate that the optical contrasts are influenced slightly by intermolecular interactions. In other words, the impact of the surroundings on α and β is similar in both the **4A**−**E** and **4A**−**K** crystals, leading to optical switching properties very close to those of the isolated compound. On the other hand, the optical contrasts calculated for **4P** show small variations when going from the isolated molecule to the unit cell, but evolves more significantly when going from the unit cell to the crystal, demonstrating the importance of the intermolecular interactions beyond the unit cell, in addition to the impact of the relative orientation of the molecules in the unit cell. In particular, the first hyperpolarizability contrast in **4P** reaches 4.55 when considering the LC-BLYP values, and it is even more pronounced (6.18) at the HF level. Therefore, contrary to **4A**, in which the β contrast upon switching is weak, the **4P** crystal should behave as a very efficient NLO switch, because of supramolecular interactions that enhance the NLO response of the keto form.

The next step was to consider the **4A**/**4P** ratio for the second-order NLO responses of the most stable enol form, as a function of the model. So, taking the LC-BLYP data as an illustration, the β_{xxx}(**4A**)/ β_{zzz}(**4P**) ratio amounts to −5.2 for the isolated molecules. For the unit cell, the corresponding ratio decreases to −3.3, whereas in the crystal $\chi^{(2)}_{uuu}$(**4A**)/$\chi^{(2)}_{uuu}$(**4P**) = −7.8, in good agreement with experiments.[7]

■ ASSOCIATED CONTENT

Supporting Information. Analysis of the $\chi^{(1)}$ and $\chi^{(2)}$ values, as a function of the method of calculation (distribution scheme and level of approximation). Molecular (hyper)polarizabilities, as a function of the method of calculation. This material is available free of charge via the Internet at http://pubs.acs.org.

■ AUTHOR INFORMATION

Corresponding Author

*Tel.: 32 81 724554. Fax: 32 81 724554. E-mail: benoit.champagne@fundp.ac.be.

Present Addresses

[§]PSE Division, KAUST, Thuwal 23955−6900, Saudi Arabia.

■ ACKNOWLEDGMENT

A.P. is grateful to the F.R.I.A. ("Fonds pour la Formation à la Recherche dans l'Industrie et dans l'Agriculture") for financial support. M.B.K. thanks the Facultés Universitaires Notre-Dame de la Paix (FUNDP, Namur, Belgium), for his CERUNA postdoctoral grant. V.L. thanks the Fund for Scientific Research (FNRS) for his postdoctoral researcher position. This work has also been supported by the academy Louvain (ARC "Extended-π Conjugated Molecular Tinkertoys for optoelectronics and spintronics") and the Belgian Government (IUAP No P06-27 "Functional

Supramolecular Systems"). The calculations were performed on the Interuniversity Scientific Computing Facility (ISCF) installed at the FUNDP, for which we gratefully acknowledge financial support from the FRS-FRFC (Convention No. 2.4.617.07.F), and the FUNDP.

REFERENCES

(1) (a) Kawata, S.; Kawata, Y. *Chem. Rev.* **2000**, *100*, 1777. (b) Bouas-Laurent, H.; Durr, H. *Pure Appl. Chem.* **2001**, *73*, 639. (b) Ferringa, B. L. *Molecular Switches*; Wiley−VCH: Weinheim, Germany, 2001. (c) Irie, M.; Fukaminato, T.; Sasaki, T.; Tamai, N.; Kawai, T. *Nature* **2002**, *470*, 759. (d) Raymo, F.; Tomasulo, M. *Chem.—Eur. J.* **2006**, *12*, 3186. (e) Gust, D.; Moore, T. A.; Moore, A. L. *Chem. Commun.* **2006**, 1169. (f) de Silva, A. P.; Vance, T. P.; West, M. E. S.; Wright, G. D. *Org. Biomol. Chem.* **2008**, *6*, 2468.

(2) (a) Coe, B. *Chem.—Eur. J.* **1999**, *5*, 2464. (b) Delaire, J. A.; Nakatani, K. *Chem. Rev.* **2000**, *100*, 1817.

(3) (a) Gilat, S. L.; Kawaï, S. H.; Lehn, J.-M. *Chem.—Eur. J.* **1995**, *1*, 275. (b) Coe, B.; Houbrechts, S.; Asselberghs, I.; Persoons, A. *Angew. Chem., Int. Ed.* **1999**, *38*, 366. (c) Asselberghs, I.; Clays, K.; Persoons, A.; Ward, M. D.; McCleverty, J. *J. Mater. Chem.* **2004**, *14*, 2831. (d) Sanguinet, L.; Pozzo, J. L.; Rodriguez, V.; Adamietz, F.; Castet, F.; Ducasse, L.; Champagne, B. *J. Phys. Chem. B* **2005**, *109*, 11139. (e) Lamère, J. F.; Lacroix, P. G.; Farfan, N.; Rivera, J. M.; Santillan, R.; Nakatani, K. *J. Mater. Chem.* **2006**, *16*, 2913. (f) Oliva, M. M.; Casado, J.; Lopez Navarrete, J. T.; Hennrich, G.; Ruiz Delgado, M. C.; Orduna, J. *J. Phys. Chem. C* **2007**, *111*, 18778. (g) Aubert, V.; Guerchais, V.; Ishow, E.; Hoang-Thi, K.; Ledoux, I.; Nakatani, K.; Le Bozec, H. *Angew. Chem., Int. Ed.* **2008**, *47*, 577. (h) Boubekeur-Lecaque, L.; Coe, B. J.; Clays, K.; Foerier, S.; Verbiest, Th.; Asselberghs, I. *J. Am. Chem. Soc.* **2008**, *130*, 3286. (i) Plaquet, A.; Guillaume, M.; Castet, F.; Ducasse, L.; Pozzo, J. L.; Rodriguez, V. *Phys. Chem. Chem. Phys.* **2008**, *10*, 6223. (j) Mançois, F.; Pozzo, J. L.; Pan, J.; Adamietz, F.; Rodriguez, V.; Ducasse, L.; Castet, F.; Plaquet, A.; Champagne, B. *Chem.—Eur. J.* **2009**, *15*, 2560.

(4) (a) Mighell, A. D.; Himes, V. L.; Rodgers, J. R. *Acta Crystallogr., Sect. A: Found Crystallogr.* **1983**, *39*, 737. (b) Bailey, R. T.; Bourhill, G.; Cruickshank, F. R.; Pug, D. J.; Sherwood, N.; Simpson, G. S. *J. Appl. Phys.* **1993**, *73*, 1591. (c) Meier, U.; Bosch, M.; Bosshard, C.; Pan, F.; Günter, P. *J. Appl. Phys.* **1998**, *83*, 3486. (d) Meier, U. *Synth. Met.* **2000**, *109*, 19. (e) Jazbinsek, M.; Mutter, L.; Günter, P. *IEEE J. Select. Top. Quantum Electron.* **2008**, *14*, 1298. (f) Kwon, O.-P.; Kwon, S. J.; Jazbinsek, M.; Brunner, F. D. J.; Seo, J.; Hunziker, C.; Schneider, A.; Yun, H.; Lee, Y.-S.; Günter, P. *Adv. Funct. Mater.* **2008**, *18*, 3242. (g) Hunziker, C.; Kwon, S.-J.; Figi, H.; Juvalta, F.; Kwon, O.-P.; Jazbinsek, M.; Günter, P. *J. Opt. Soc. Am. B* **2008**, *25*, 1678. (h) Luo, S. J.; Du, W. F.; Wang, H. Z. *J. Chem. Phys.* **2008**, *129*, 094705. (i) Kwon, O.-P.; Jazbinsek, M.; Seo, J.-I.; Choi, E.-Y.; Yun, H.; J. Brunner, F. D. J.; Lee, Y. S.; Günter, P. *J. Chem. Phys.* **2009**, *130*, 134708. (j) Kwon, O.-P.; Kwon, S. J.; Jazbinsek, M.; Seo, J.-Y.; Kim, J. T.; Seo, J. I.; Lee, Y. S.; Yun, H.; Günter, P *Chem. Mater.* **2011**, *23*, 239.

(5) Levine, B. F.; Bethea, C. G.; Thurmond, C. D.; Lynch, R. T. *J. Appl. Phys.* **1979**, *50*, 2523.

(6) Kanis, D. R.; Ratner, M. A.; Marks, T. J. *Chem. Rev.* **1994**, *94*, 195–242.

(7) Sliwa, M.; Létard, S.; Malfant, I.; Nierlich, M.; Lacroix, P. G.; Asahi, T.; Masuhara, H.; Yu, P.; Nakatani, K. *Chem. Mater.* **2005**, *17*, 4727–4735.

(8) (a) Sliwa, M.; Nakatani, K.; Asahi, T.; Lacroix, P. G.; Pansu, R. B.; Masuhara, H. *Chem. Phys. Lett.* **2007**, *437*, 212. (b) Sliwa, M.; Mouton, N.; Ruckebusch, C.; Aloïse, S.; Poizat, O.; Buntinx, G.; Métivier, R.; Nakatani, K.; Masuhara, H.; Asahi, T. *J. Phys. Chem. C* **2009**, *113* (27), 11959.

(9) (a) Plaquet, A.; Guillaume, M.; Champagne, B.; Rougier, L.; Mançois, F.; Rodriguez, V.; Pozzo, J. L.; Ducasse, L.; Castet, F. *J. Phys. Chem. C* **2008**, *112*, 5638. (b) Bogdan, E.; Plaquet, A.; Antonov, L.; Rodriguez, V.; Ducasse, L.; Champagne, B.; Castet, F. *J. Phys. Chem. C* **2010**, *114*, 12760.

(10) Champagne, B.; Bishop, D. M. *Adv. Chem. Phys.* **2003**, *126*, 41.

(11) (a) Chemla, D. S.; Oudar, J. L.; Jerphagnon, J. *J. Phys. Rev. B* **1975**, *12*, 4534. (b) Zyss, J.; Oudar, J. L. *Phys. Rev. A* **1982**, *26*, 2028.

(12) (a) Guillaume, M.; Botek, E.; Champagne, B.; Castet, F.; Ducasse, L. *J. Chem. Phys.* **2004**, *121*, 7390. (b) Botek, E.; Giribet, C.; Ruiz de Azua, M.; Negri, R. M.; Bernik, D. *J. Phys. Chem. A* **2008**, *112*, 6992. (c) Holtmann, J.; Walczuk, E.; Dede, M.; Wittenburg, C.; Heck, J.; Archetti, G.; Wortmann, R.; Kuball, H. G.; Wang, Y. H.; Liu, K.; Luo, Y. *J. Phys. Chem. B* **2008**, *112*, 14751. (d) Zhao, K.; Tu, Y.; Luo, Y. *J. Phys. Chem. B* **2009**, *113*, 10271.

(13) (a) Darrigan, C.; Rérat, M.; Mallia, G.; Dovesi, R. *J. Comput. Chem.* **2003**, *24*, 1305. (b) Veithen, M.; Gonze, X.; Ghosez, Ph. *Phys. Rev. Lett.* **2004**, *93*, 187401. (c) Ferrero, M.; Rérat, M.; Orlando, R.; Dovesi, R. *J. Comput. Chem.* **2008**, *29*, 1450. (d) Ferrero, M.; Rérat, M.; Kirtman, B.; Dovesi, R. *J. Chem. Phys.* **2008**, *129*, 244110. (e) Kirtman, B.; Ferrero, M.; Rérat, M.; Springborg, M. *J. Chem. Phys.* **2009**, *131*, 044109. (f) Ferrero, M.; Civalleri, B.; Rérat, M.; Orlando, R.; Dovesi, R. *J. Chem. Phys.* **2009**, *131*, 214704. (g) Hermet, P.; Ghosez, Ph. *Phys. Chem. Chem. Phys.* **2010**, *12*, 835.

(14) (a) Munn, R. W. *Chem. Phys.* **1980**, *50*, 119. (b) Hurst, M.; Munn, R. W. *J. Mol. Electron.* **1986**, *2*, 101.

(15) (a) Dunmur, D. A. *Mol. Phys.* **1972**, *23*, 109. (b) Cummins, P. G.; Dunmur, D. A.; Munn, R. W.; Newham, R. J. *Acta Crystallogr., Sect. A: Cryst. Phys., Diffr., Theor. Gen. Crystallogr.* **1976**, *A32*, 847. (c) Cummins, P. G.; Dunmur, D. A.; Munn, R. W.; Newham, R. J. *Acta Crystallogr., Sect. A: Cryst. Phys., Diffr., Theor. Gen. Crystallogr.* **1976**, *A32*, 854.

(16) (a) Kirtman, B.; Dykstra, C. E.; Champagne, B. *Chem. Phys. Lett.* **1999**, *305*, 132. (b) Reis, H.; Papadopoulos, M. G.; Calaminici, P.; Jug, K.; Köster, A. M. *Chem. Phys.* **2000**, *261*, 359. (c) Reis, H.; Makowska-Janusika, M.; Papadopoulos, M. G. *J. Phys. Chem. B* **2004**, *108*, 8931. (c) Spackman, M. A.; Munshi, P.; Jayatilaka, D. *Chem. Phys. Lett.* **2007**, *443*, 87. (d) Jayatilaka, D.; Munshi, P.; Turner, M. J.; Howard, J. A. K.; Spackman, M. A. *Phys. Chem. Chem. Phys.* **2009**, *11*, 7209. (e) Mayer, A.; Gonzalez, A. L.; Aitkens, C. M.; Schatz, G. C. *Nanotechnology* **2009**, *20*, 195204. (f) Kanoun, M. B.; Botek, E.; Champagne, B. *Chem. Phys. Lett.* **2010**, *487*, 256.

(17) (a) Sekino, H.; Bartlett, R. J. *J. Chem. Phys.* **1986**, *85*, 976. (b) Karna, S. P.; Dupuis, M. *J. Comput. Chem.* **1991**, *12*, 487.

(18) (a) Leininger, T.; Stoll, H.; Werner, H.-J.; Savin, A. *Chem. Phys. Lett.* **1997**, *275*, 151. (b) Iikura, H.; Tsuneda, T.; Yanai, T.; Hirao, K. *J. Chem. Phys.* **2001**, *115*, 3540.

(19) (a) Kamiya, M.; Sekino, H.; Tsuneda, T.; Hirao, K. *J. Chem. Phys.* **2005**, *122*, 234111. (b) Kirtman, B.; Bonness, S.; Ramirez-Solis, A.; Champagne, B.; Matsumoto, H.; Sekino, H. *J. Chem. Phys.* **2008**, *128*, 114108.

(20) (a) Runge, E.; Gross, E. K. U. *Phys. Rev. Lett.* **1984**, *52*, 997. (b) Bauernschmitt, R.; Ahlrichs, R. *Chem. Phys. Lett.* **1996**, *256*, 454.

(21) (a) Cohen, H. D.; Roothaan, C. C. J. *J. Chem. Phys.* **1965**, *43*, S34. (b) For an application of this method and the use of Romberg procedure, see:Champagne, B.; Kirtman, B. In *Handbook of Advanced Electronic and Photonic Materials and Devices*; Nalwa, H. S., Ed.; Academic Press: New York, 2001; Vol. 9, Chapter 2, p 63.

(22) Frisch, M. J.; Trucks, G. W.; Schlegel, H. B.; Scuseria, G. E.; Robb, M. A.; Cheeseman, J. R.; Montgomery, J. A.; Vreven, T.; Kudin, K. N.; Burant, J. C.; Millam, J. M.; Iyengar, S. S.; Tomasi, J.; Barone, V.; Mennucci, B.; Cossi, M.; Scalmani, G.; Rega, N.; Petersson, G. A.; Nakatsuji, H.; Hada, M.; Ehara, M.; Toyota, K.; Fukuda, R.; Hasegawa, J.; Ishida, M.; Nakajima, T.; Honda, Y.; Kitao, O.; Nakai, H.; Klene, M.; Li, X.; Knox, J. E.; Hratchian, H. P.; Cross, J. B.; Bakken, V.; Adamo, C.; Jaramillo, J.; Gomperts, R.; Stratmann, R. E.; Yazyev, O.; Austin, A. J.; Cammi, R.; Pomelli, C.; Ochterski, J. W.; Ayala, P. Y.; Morokuma, K.; Voth, G. A.; Salvador, P.; Dannenberg, J. J.; Zakrzewski, V. G.; Dapprich, S.; Daniels, A. D.; Strain, M. C.; Farkas, O.; Malick, D. K.; Rabuck, A. D.; Raghavachari, K.; Foresman, J. B.; Ortiz, J. V.; Cui, Q.; Baboul, A. G.; Clifford, S.; Cioslowski, J.; Stefanov, B. B.; Liu, G.; Liashenko, A.; Piskorz, P.; Komaromi, I.; Martin, R. L.; Fox, D. J.; Keith, T.; Al-Laham, M. A.; Peng, C. Y.; Nanayakkara, A.; Challacombe, M.; Gill, P. M. W.; Johnson, B.; Chen, W.; Wong, M. W.; Gonzalez, C.; Pople, J. A. *Gaussian 09, Revision A.02*; Gaussian, Inc.: Wallingford, CT, 2009.

(23) Frisch, M. J.; Trucks, G. W.; Schlegel, H. B.; Scuseria, G. E.; Robb, M. A.; Cheeseman, J. R.; Montgomery, J. A.; Vreven, T.; Kudin, K. N.; Burant, J. C.; Millam, J. M.; Iyengar, S. S.; Tomasi, J.; Barone, V.; Mennucci, B.; Cossi, M.; Scalmani, G.; Rega, N.; Petersson, G. A.; Nakatsuji, H.; Hada, M.; Ehara, M.; Toyota, K.; Fukuda, R.; Hasegawa, J.; Ishida, M.; Nakajima, T.; Honda, Y.; Kitao, O.; Nakai, H.; Klene, M.; Li, X.; Knox, J. E.; Hratchian, H. P.; Cross, J. B.; Bakken, V.; Adamo, C.; Jaramillo, J.; Gomperts, R.; Stratmann, R. E.; Yazyev, O.; Austin, A. J.; Cammi, R.; Pomelli, C.; Ochterski, J. W.; Ayala, P. Y.; Morokuma, K.; Voth, G. A.; Salvador, P.; Dannenberg, J. J.; Zakrzewski, V. G.; Dapprich, S.; Daniels, A. D.; Strain, M. C.; Farkas, O.; Malick, D. K.; Rabuck, A. D.; Raghavachari, K.; Foresman, J. B.; Ortiz, J. V.; Cui, Q.; Baboul, A. G.; Clifford, S.; Cioslowski, J.; Stefanov, B. B.; Liu, G.; Liashenko, A.; Piskorz, P.; Komaromi, I.; Martin, R. L.; Fox, D. J.; Keith, T.; Al-Laham, M. A.; Peng, C. Y.; Nanayakkara, A.; Challacombe, M.; Gill, P. M. W.; Johnson, B.; Chen, W.; Wong, M. W.; Gonzalez, C.; Pople, J. A. *Gaussian 03, Revision C.02*; Gaussian, Inc.: Wallingford, CT, 2004.

(24) X-ray crystallographic data for **4A** and **4P** are available free of charge via the Internet at http://pubs.acs.org. Deposited Data: CCDC 261613 and 261614.

(25) Sliwa, M.; Nakatani, K.; Masuhara, H. *Mol. Cryst. Liq. Cryst.* **2005**, *431*, 241.

(26) (a) Suponitsky, K. Y.; Tafur, S.; Masunov, A. E. *J. Chem. Phys.* **2008**, *129*, 044109. (b) Limacher, P. A.; Mikkelsen, K. V.; Lüthi, H. P. *J. Chem. Phys.* **2009**, *130*, 194114. (c) de Wergifosse, M.; Champagne, B. *J. Chem. Phys.* **2011**, *134*, 074113.